Stratospheric Harbingers of Anomalous Weather Regimes

Mark P. Baldwin, *et al.*

Science **294**, 581 (2001);
DOI: 10.1126/science.1063315

Stratospheric Harbingers of Anomalous Weather Regimes

Mark P. Baldwin* and Timothy J. Dunkerton

Observations show that large variations in the strength of the stratospheric circulation, appearing first above ~50 kilometers, descend to the lowermost stratosphere and are followed by anomalous tropospheric weather regimes. During the 60 days after the onset of these events, average surface pressure maps resemble closely the Arctic Oscillation pattern. These stratospheric events also precede shifts in the probability distributions of extreme values of the Arctic and North Atlantic Oscillations, the location of storm tracks, and the local likelihood of mid-latitude storms. Our observations suggest that these stratospheric harbingers may be used as a predictor of tropospheric weather regimes.

Tropospheric weather patterns tend to change on time scales of a few days, and numerical prediction models have little skill beyond a week. On a time scale of months—in several parts of the world—predictive skill comes from El Niño/Southern Oscillation. Circulation regimes in the stratosphere tend to persist for several weeks or more, but the stratospheric circulation is generally regarded as having little influence on surface weather patterns. Case studies have shown, however, that large stratospheric circulation anomalies occasionally reach Earth's surface (*1*, *2*).

The stratospheric circulation is most variable during winter, when the cold, cyclonic polar vortex varies in strength and is disturbed by planetary-scale Rossby waves. These waves originate mainly in the troposphere and transport westward angular momentum upward, where they interact with the stratospheric flow. The longitudinally averaged wind, $\bar{u}$, modulates the refraction of upward-propagating planetary-scale waves (*3*), alters the locations where the angular momentum is changed, and can initiate a positive feedback in which the waves penetrate to successively lower altitudes (*4*–*6*) as $\bar{u}$ anomalies descend.

Wave-induced angular momentum transport, driven by upward-propagating waves, thus leads to downward phase propagation of $\bar{u}$ anomalies. The downward phase propagation creates what may be an illusion of downward influence, especially when the data are smoothed in time. Downward phase propagation does not in itself imply that anomalies at lower levels originate at upper levels. Rather, it seems more likely that the stratosphere is modified by waves originating in the troposphere, altering the conditions for planetary-wave propagation in such a way as to draw mean-flow anomalies poleward and downward (*7*).

Here we use daily stratospheric weather maps to identify large stratospheric circulation anomalies. We then examine time averages and variability of the near-surface circulation during 60-day periods after the onset of these anomalies. This methodology makes it clear that large stratospheric anomalies precede tropospheric mean-flow anomalies and may therefore be useful for tropospheric weather prediction. From the observed time delay—and on the basis of independent modeling evidence—we speculate that the stratospheric anomalies may also have a causal role in creating the subsequent tropospheric anomalies.

Variations in the strength of the polar vortex are well characterized by "annular modes," which are hemispheric-scale patterns characterized by synchronous fluctuations in pressure of one sign over the polar caps and of opposite sign at lower latitudes. We use daily November to April data (*8*) to define the annular mode independently at each of 26 pressure altitudes from 1000 to 0.316 hPa (*9*). At each pressure altitude the annular mode is the first empirical orthogonal function (EOF) of 90-day low-pass filtered geopotential anomalies north of 20°N (*10*, *11*). Daily values of the annular mode, spanning the entire 42-year data record, are calculated for each pressure altitude by projecting daily geopotential anomalies onto the leading EOF patterns. Annular modes provide a somewhat better measure of vertical coupling than longitudinally averaged fields such as $\bar{u}$ (*12*). In the stratosphere annular mode values are a measure of the strength of the polar vortex, while the near-surface annular mode is called the "Arctic Oscillation" (AO) (*13*), which is recognized as the North Atlantic Oscillation (NAO) (*14*, *15*) over the Atlantic sector.

The northern winter of 1998–1999 (Fig. 1) illustrates the time-height development of the annular mode, shown with daily resolution. In the stratosphere the time scale is relatively long, illustrating periods when the polar vortex was warm and weak (red), beginning in December and late February, and periods when the polar vortex was cold and strong (blue). Large anomalies tend to appear first at the top of the diagram, and move downward (*16*). The time scale in the troposphere is much shorter, and variations are often distinct from those in the stratosphere. Other winters during 1958–1999 have descending positive and negative anomalies that often appear to reach Earth's surface, but not all events behave in this way. In general, only the strongest anomalies of either sign tend to connect to the surface, while weaker anomalies typically remain within the stratosphere. There are also exceptions in which tropospheric anomalies appear to precede stratospheric anomalies.

We now examine composites (averages) of large negative anomalies and large positive anomalies, as measured by the 10-hPa annular mode values (*17*). These daily values are highly correlated (0.95) with $\bar{u}$ at 10 hPa, 60°N. Large positive values represent a strong, well-organized vortex, while large negative values represent a weak, disorganized vortex (*18*). We define weak and strong vortex "events" by the dates on which the 10-hPa annular mode values (which are negatively skewed) crossed the thresholds of −3.0 and +1.5, respectively, while increasing in magnitude. We choose these values so that the average event is sufficiently strong to reach the troposphere, while capturing enough events to obtain a meaningful composite. ("Event" therefore refers to the onset of a large stratospheric circulation anomaly. Later, we use "regime" to denote an extended period of time after the onset of the stratospheric anomaly.) The results are not sensitive to the exact threshold values. In practice, the crossing of the threshold could be determined operationally from 10-hPa weather maps or from numerical forecasts. There were 18 weak vortex events (*19*) and 30 strong vortex events, with the highest concentration during December to February (*20*). Composites of these extreme events (Fig. 2) show that circulation anomalies descend from 10 hPa to the lower stratosphere where they persist, on average, for more than 2 months. The anomalies at 10 hPa do not last as long as those in the lower stratosphere where the radiative time scale is longer (*21*).

In the weak vortex composite (Fig. 2A) the stratospheric vortex is very weak at lag zero (when the 10-hPa values exceeded −3.0), yet the AO index (at 1000 hPa) is near zero. On average it takes about 10 days for the phase of annular mode to descend to near the tropopause. Although the 10-hPa values are positive after day 40, the negative anomaly just above the tropopause lasts more than 60 days, during which time the tropospheric vortex tends to be weaker than normal (red). The short-period tropospheric fluctuations within the 60 days after the events in Fig. 2 are probably not meaningful. The composite for the strong vortex events (Fig. 2B) is similar, but with a longer delay at the surface until the AO index becomes strongly positive (blue).

Northwest Research Associates, 14508 Northeast 20th Street, Bellevue, WA 98007–3713, USA.

*To whom correspondence should be addressed. E-mail: mark@nwra.com

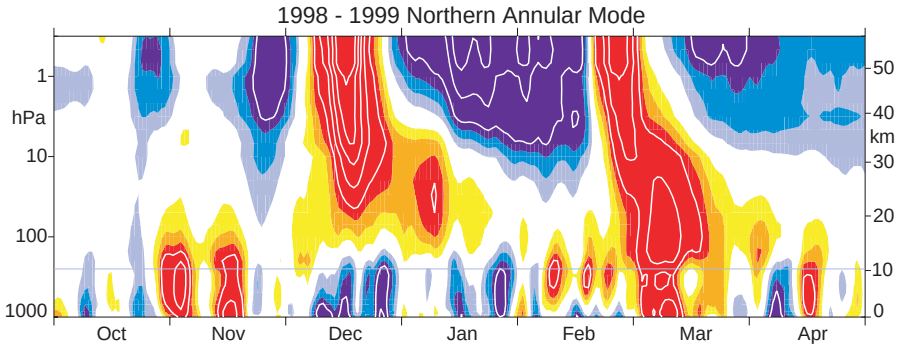

Fig. 1. Time-height development of the northern annular mode during the winter of 1998–1999. The indices have daily resolution and are nondimensional. Blue corresponds to positive values (strong polar vortex), and red corresponds to negative values (weak polar vortex). The contour interval is 0.5, with values between −0.5 and 0.5 unshaded. The thin horizontal line indicates the approximate boundary between the troposphere and the stratosphere.

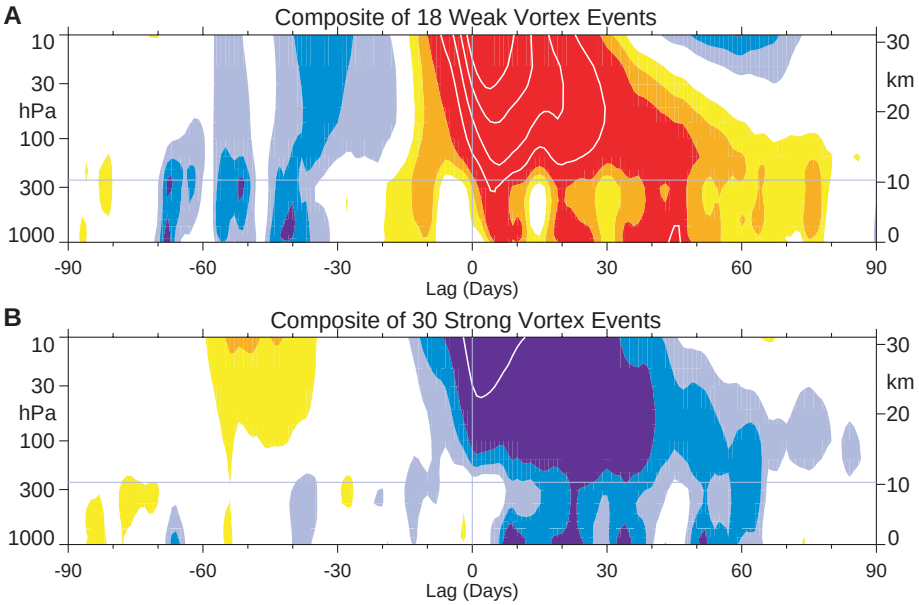

Fig. 2. Composites of time-height development of the northern annular mode for (**A**) 18 weak vortex events and (**B**) 30 strong vortex events. The events are determined by the dates on which the 10-hPa annular mode values cross –3.0 and +1.5, respectively. The indices are nondimensional; the contour interval for the color shading is 0.25, and 0.5 for the white contours. Values between −0.25 and 0.25 are unshaded. The thin horizontal lines indicate the approximate boundary between the troposphere and the stratosphere.

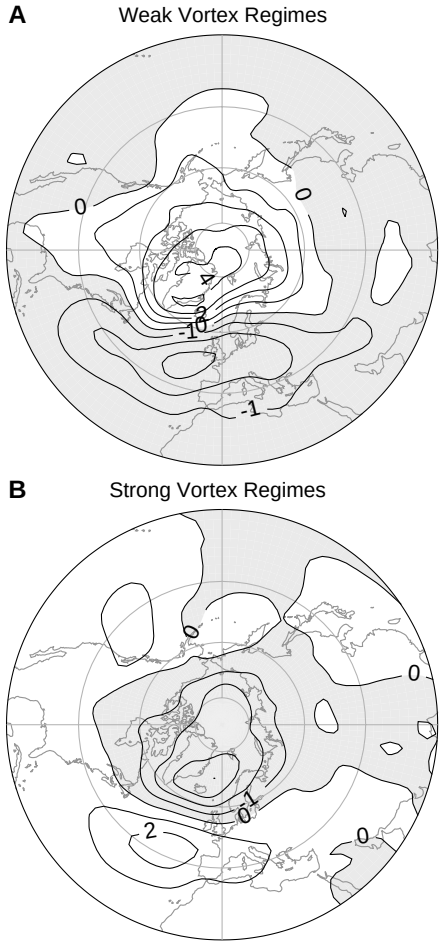

Fig. 3. Average sea-level pressure anomalies (hPa) for (**A**) the 1080 days during weak vortex regimes and (**B**) the 1800 days during strong vortex regimes.

Stratospheric and tropospheric annular mode variations are sometimes independent of each other, but (on average) strong anomalies just above the tropopause appear to favor tropospheric anomalies of the same sign. Opposing anomalies as in December 1998 (Fig. 1) are possible, but anomalies of the same sign dominate the average (Fig. 2).

To examine the tropospheric circulation after these extreme events, we define weak and strong vortex "regimes" as the 60-day periods after the dates on which the −3.0 and +1.5 thresholds were crossed. Our results are not sensitive to the exact range of days used and do not depend on the first few days after the "events." We focus on the average behavior during these "weak vortex regimes" and "strong vortex regimes," as characterized by the normalized AO index (*22*). The average value (1080 days) during weak vortex regimes is −0.44, and +0.35 for strong vortex regimes (1800 days). The large sample sizes contribute to the high statistical significance of these averages (*23*). During the weak and strong vortex regimes the average surface pressure anomalies (Fig. 3) are markedly like opposite phases of the AO (*11*) or NAO (*14*), with the largest effect on pressure gradients in the North Atlantic and Northern Europe.

The probability density functions (PDFs) of the daily normalized AO and NAO indices (*24*) during weak and strong vortex regimes are compared in Fig. 4. More pronounced than the shift in means are differences in the shapes of the PDFs, especially between the tails of the curves. Values of AO or NAO index greater than 1.0 are three to four times as likely during strong vortex regimes than weak vortex regimes. Similarly, index values less than −1.0 are three to four times as likely during weak vortex regimes than strong vortex regimes. Values of the daily AO index greater than 1.0 and less than −1.0 are associated with statistically significant changes in the probabilities of weather extremes such as cold air outbreaks, snow, and high winds across Europe, Asia, and North America (*25*). The observed circulation changes during weak and strong vortex regimes are substantial from a meteorological viewpoint and can be anticipated by observing the stratosphere. These results imply a measure of predictability, up to 2 months in advance, for AO/NAO variations in northern winter, particularly for extreme values that are associated with unusual weather events having the greatest impact on society.

Since the NAO and AO are known to modulate the position of surface cyclones across the Atlantic and Europe, we examine the tracks of surface cyclones with central pressure less than

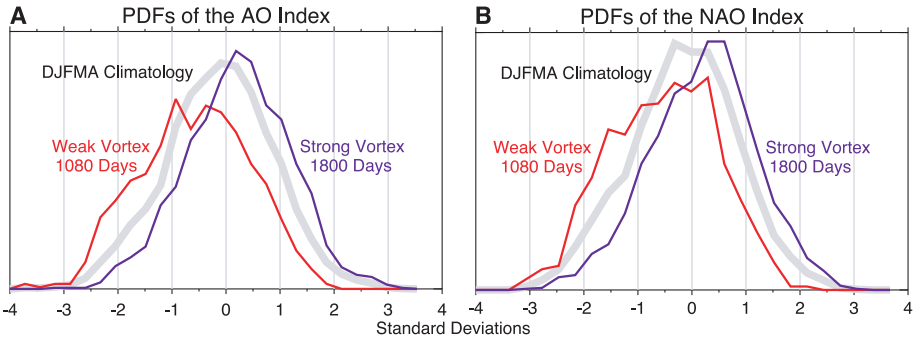

Fig. 4. (**A**) Probability density function for the normalized daily AO index during December to April (gray curve), the 1080 days during weak vortex regimes (red curve), and the 1800 days during strong vortex regimes (blue curve). (**B**) As in (A), but for the NAO index.

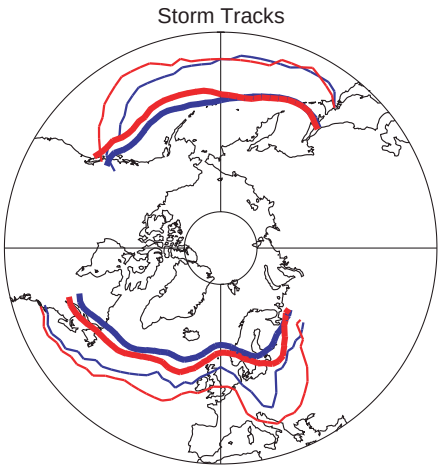

Fig. 5. Average latitudes of surface cyclones (defined as closed low-pressure centers less than 1000 hPa) in the Atlantic and Pacific sectors for the 1080 days during weak vortex regimes (thick red lines) and the 1800 days during strong vortex regimes (thick blue lines). The thin lines indicate the lowest latitude at which a cyclone frequency of one per two weeks is expected. The data span 1961–1998, and each data point represents the average of a 15° band in longitude.

1000 hPa (*26*) during weak and strong vortex regimes (Fig. 5). Over the Atlantic sector, the storm track is displaced significantly (*27*) farther south during weak vortex regimes, compared with strong vortex regimes. We also find a similar effect in the eastern Pacific, a result that would not be expected from modulation of the NAO, but is consistent with hemispheric modulation of weather events by the AO (*25*). The thin lines illustrate the minimum latitude at which one storm is expected per 2 weeks, with storms more frequent to the north. The difference between weak and strong vortex regimes, particularly across the United Kingdom and central and southern Europe, is statistically significant (*28*); storms are more likely during weak vortex regimes than strong vortex regimes.

Although stratospheric circulation anomalies are believed to be caused mainly by upward-propagating planetary-scale waves, other processes within the stratosphere may affect the likelihood of extreme events and subsequent changes in surface weather. The quasi-biennial oscillation (QBO) in the equatorial stratosphere (*29*) modulates the wave guide for upward-propagating planetary waves so that major stratospheric warmings are less likely when the equatorial stratospheric winds are westerly (*30*). In our analysis, weak vortex regimes are twice as likely (12/6) when the QBO (*31*) is easterly, and strong vortex regimes are almost three times as likely (22/8) when the QBO is westerly. Because the phase of the QBO can be anticipated up to a year in advance, this result implies a degree of long-range predictability (*32*).

Persistent circulation anomalies in the lower stratosphere evidently favor tropospheric anomalies of the same sign, but the mechanism involved is not completely clear. Circulation anomalies with large spatial scales in the lowermost stratosphere are expected to induce changes in the troposphere, but this effect is difficult to quantify (*33*, *34*). Possible mechanisms responsible for this coupling include (i) a mean meridional circulation induced by planetary wave drag in the lowermost stratosphere, with open streamlines at the surface (*35*), and (ii) critical layer absorption in the polar lower troposphere of Rossby waves that have been reflected downward from the stratosphere. We have explored the role of these mechanisms using a three-dimensional primitive equation model in a separate investigation (*36*). Our numerical experiments indicate that planetary-wave variations of heat and momentum flux—corresponding to anomalies in wave propagation associated with stratospheric mean-flow variations—induce variations in mean meridional circulation that penetrate the lower troposphere. Coriolis torques associated with these circulation anomalies cause tropospheric $\bar{u}$ and surface pressure anomalies similar to those observed in the present study. These numerical results indicate that it is primarily the induced circulation mechanism, rather than the tropospheric absorption of reflected waves, that is responsible for vertical coupling to the surface. However, it will be necessary to explore the parameter space more thoroughly in order to generalize this result to the real atmosphere.

Our observations suggest that large circulation anomalies in the lower stratosphere are related to substantial shifts in the AO/NAO and that these stratospheric signals may be used as a predictive tool. Our results further suggest the possibility that other changes to the stratosphere (e.g., from volcanic aerosols, solar irradiance, or greenhouse gases) could in turn be related to surface weather if they affect the likelihood or timing of extreme circulation events in the polar lower stratosphere (*37*).

References and Notes

1. P. R. Julian, K. B. Labitzke, *J. Atmos. Sci.* **22**, 597 (1965).
2. R. S. Quiroz, *Geophys. Res. Lett.* **4**, 151 (1977).
3. Local longitudinal flow anomalies of sufficient scale may also be enough to substantially modulate refraction.
4. J. R. Holton, C. F. Mass, *J. Atmos. Sci.* **33**, 2218 (1976).
5. T. J. Dunkerton, C.-P. F. Hsu, M. E. McIntyre, *J. Atmos. Sci.* **38**, 819 (1981).
6. D. T. Shindell, G. A. Schmidt, R. L. Miller, D. Rind, *J. Geophys. Res.* **106**, 7193 (2001).
7. T. J. Dunkerton, *J. Atmos. Sci.* **57**, 3838 (2000).
8. National Centers for Environmental Prediction (NCEP) reanalysis data for 1000 to 10 hPa during 1958–1999, supplemented with Tiros Operational Vertical Sounder data up to 1 hPa during 1979–1993, and UK Meteorological Office data up to 0.316 hPa during 1993–1999. All data were on a 2.5° longitude by 2.5° latitude grid. The NCEP reanalysis data were obtained from the National Oceanic and Atmospheric Administration–Cooperative Institute for Research in Environmental Sciences (NOAA-CIRES) Climate Diagnostics Center.
9. Hectopascals, equal to millibars. The altitude range is from the surface to ~57 km.
10. We calculate the annular mode as follows. For each pressure altitude we calculate the seasonally varying climatology as the (90-day low-pass filtered) average at each latitude, longitude, pressure altitude, and day of year. The climatology (seasonal cycle) is then subtracted, leaving anomalies. The anomaly fields retain variations on daily to interannual time scales, but the seasonal cycle has been removed. We then apply a 90-day low-pass filter to the anomaly fields and retain only November to April data from 20°N to the North Pole. After weighting the data by the square root of the cosine of latitude, we calculate the leading EOF spatial pattern and EOF time series. The annular mode patterns are defined as the regression between the EOF time series and the data field used in the EOF calculation. A separate EOF calculation is made for each pressure altitude, unlike (*12*), in which a single EOF calculation spanned pressure altitudes from 1000 to 10 hPa.
11. A supplementary Web figure of the annular mode patterns is available on *Science* Online at www.sciencemag.org/cgi/content/full/294/5542/581/DC1.
12. M. P. Baldwin, T. J. Dunkerton, *J. Geophys. Res.* **104**, 30937 (1999).
13. D. W. J. Thompson, J. M. Wallace, *Geophys. Res. Lett.* **25**, 1297 (1998).
14. J. W. Hurrell, *Science* **269**, 676 (1995).
15. J. M. Wallace, *Q. J. R. Meteorol. Soc.* **126**, 791 (2000).
16. There is a certain visual resemblance between Fig. 1 and the quasi-biennial oscillation (QBO) in the equatorial stratosphere with its downward-propagating regimes of easterly and westerly wind. The wave-induced momentum transport during the descent of the negative (red) anomalies is similar to that which drives the QBO: upward-propagating waves cause the descent of mean wind regimes. In the QBO, however, both phases are forced by a broad spectrum of equatorial waves, while in the present case, the

relevant waves (planetary-scale Rossby waves) are primarily responsible for deceleration of westerlies. These waves, moreover, are far greater in vertical scale and not accurately described by the kind of slow-modulation wave theory used in models of the QBO.
17. Ten hPa is the highest pressure altitude available for all of 1958–1999.
18. N. P. Gillett, M. P. Baldwin, M. R. Allen, *J. Geophys. Res.* **105**, 7891 (2001).
19. The weak vortex events correspond closely to major stratospheric warmings, in which the normal westerly winds are replaced by easterlies at high latitudes.
20. The earliest event occurred 26 November and the latest on 23 March.
21. K. P. Shine, *Q. J. R. Meteorol. Soc.* **113**, 603 (1987).
22. The AO index was normalized by the standard deviation of daily values during December to April.
23. Monte Carlo simulations with 18 randomly selected 60-day periods beginning during December to February indicate that a mean value less than −0.44 has a probability of occurrence by chance of less than 0.003. A mean value of more than +0.35, with 30 events, also has a probability of occurrence by chance of less than 0.003.
24. We first defined the NAO spatial pattern by regressing monthly-mean 1000-hPa December to February geopotential anomalies onto Hurrell's NAO index (1958–1997). The daily NAO index is defined by projecting daily 1000-hPa geopotential anomalies onto the NAO spatial pattern. The correlation between the daily AO and NAO indices is 0.93.
25. D. W. J. Thompson, J. M. Wallace, *Science* **293**, 85 (2001).
26. From NASA's *Atlas of Extratropical Cyclones 1961–1998*.
27. Monte Carlo simulations indicate that the average latitudinal separation between the two curves (1.96°) has a probability of occurrence by chance of less than 0.001.
28. Monte Carlo simulations indicate that the average latitudinal separation between the two curves (2.94°) has a probability of occurrence by chance of less than 0.002.
29. M. P. Baldwin *et al*., *Rev. Geophys.* **39**, 179, 2001.
30. J. R. Holton, H.-C. Tan, *J. Atmos. Sci.* **37**, 2200 (1980).
31. We define the phase of the QBO by the 40-hPa equatorial wind.
32. D. W. J. Thompson, M. P. Baldwin, J. M. Wallace, in preparation.
33. W. A. Robinson, *J. Atmos. Sci.* **45**, 2319 (1988).
34. D. E. Hartley, J. T. Villarin, R. X. Black, C. A. Davis, *Nature* **391**, 471 (1998).
35. P. H. Haynes, T. G. Shepherd, *Q. J. R. Meteorol. Soc.* **115** 1181 (1989).
36. D. Ortland, T. J. Dunkerton, in preparation.
37. We thank M. A. Geller, J. R. Holton, G. N. Kiladis, M. E. McIntyre, and P. W. Mote for comments on the manuscript. Equatorial 40-hPa winds are courtesy of B. Naujokat, Freie University Berlin. Supported by the SR&T Program for Geospace Science (NASA), ACMAP Program (NASA), CLIVAR Atlantic, Office of Global Programs (NOAA), and the National Science Foundation.

11 June 2001; accepted 13 September 2001

Climatic Impact of Tropical Lowland Deforestation on Nearby Montane Cloud Forests

R. O. Lawton,[1]* U. S. Nair,[2] R. A. Pielke Sr.,[3] R. M. Welch[2]

Tropical montane cloud forests (TMCFs) depend on predictable, frequent, and prolonged immersion in cloud. Clearing upwind lowland forest alters surface energy budgets in ways that influence dry season cloud fields and thus the TMCF environment. Landsat and Geostationary Operational Environmental Satellite imagery show that deforested areas of Costa Rica's Caribbean lowlands remain relatively cloud-free when forested regions have well-developed dry season cumulus cloud fields. Further, regional atmospheric simulations show that cloud base heights are higher over pasture than over tropical forest areas under reasonable dry season conditions. These results suggest that land use in tropical lowlands has serious impacts on ecosystems in adjacent mountains.

In the Caribbean basin, as in much of the tropics, cloud forests occur where mountains force trade winds to rise above the lifting condensation level, the point of orographic cloud formation. Immersion of forest in cloud reduces solar radiation and outgoing longwave radiation, increases humidity and water inputs from mist and direct deposition of cloud droplets, and reduces transpiration (*1*, *2*). Because these actions influence soil structure, nutrient cycling, and composition of the vegetation, factors that influence the location and likelihood of cloud formation in the air masses moving over tropical mountains have profound consequences for landscape conservation and management (*1*, *3*, *4*). The Monteverde cloud forests, which are the focus of considerable conservation and research interest, provide a case in point (*2*, *5*, *6*). These lie along the crest of the Cordillera de Tilarán mountain range, which rises abruptly from the lowlands of western Costa Rica to peaks higher than 1800 m. Tropical wet forest below 700 m on the Caribbean slope grades through premontane rain forest to cloud forests at the highest elevations (*6*, *7*). The uppermost Pacific slopes are covered by lower montane wet forest, which rapidly gives way below 1500 m to a landscape that is now almost completely deforested, but was once covered with semi-evergreen premontane wet and moist forests (Fig. 1A). These transitions are largely due to the spatial pattern of dry season water inputs imposed by the orographic rise of the trade winds flowing over the Cordillera and the consequent formation of a cloud bank against the upper windward slopes (*2*, *6*, *7*). The local environmental heterogeneity produced by the geography of cloud immersion results in high levels of endemism and one of the richest floras in the world (*6*, *8*).

In the Cordillera, anuran population crashes, an increase in the upper elevation of bird ranges on the Pacific slope, and longer mist-free intervals in the dry season at the lee edge of the Monteverde cloud forest have been attributed to an increase in the base height of the orographic cloud bank (*3*). The frequency of long (≥5 days) mist-free periods in the dry season is related to Pacific sea surface temperatures, and thus to El Niño events, but a trend remains after these are considered (*3*). Based on a global climate model under $2XCO_2$ conditions, Still *et al*. (*4*) suggest that sea surface warming results in intensification of tropical hydrological cycling, with release of latent heat upon condensation, warming the atmosphere. From these results, Still *et al*. (*4*) and Pounds *et al*. (*3*) infer an increase in the lifting condensation level and the height of orographic cloud banks. Global climate models, however, have coarse spatial resolution [~400 km horizontally and several hundred meters vertically in that of Still *et al*. (*4*)] and are incapable of resolving subgrid scale features such as clouds, or terrain and land use features known to influence cloud formation.

Trade winds flow from the Caribbean, 100 km across the lowlands of the Rio San Juan basin, to the Monteverde tropical montane cloud forest (TMCF). Moving at 3 to 5 m s^{-1}, the lower atmosphere has 5 to 10 hours during which it can be influenced by the land below. Deforestation proceeded rapidly in the Costa Rican part of this basin in the past century. By 1940, a 600-km^2 area at the Caribbean foot of the Cordillera de Tilarán had been cleared (*9*). Agricultural colonization has since spread (*9*, *10*). By 1992, only about 1200 km^2 (18% of the area) of intact natural vegetation remained in the Costa Rican part of the Rio San Juan basin lowlands (*11*) (Fig. 1A). To the north of the river, the forests in southeastern Nicaragua remained largely intact.

Deforestation and conversion of land to pasture or cropland generally increase surface albedo (*12*), reduce aerodynamic roughness length and mechanically turbulent mixing in the boundary layer (*13*), reduce evapotranspiration, and increase the ratio of convective sensible

[1]Department of Biological Sciences, University of Alabama in Huntsville, Huntsville, AL 35899, USA. [2]Department of Atmospheric Science, National Space Science Technology Center, University of Alabama in Huntsville, 320 Sparkman Drive, Huntsville, AL 35806, USA. [3]Department of Atmospheric Science, Colorado State University, Fort Collins, CO 80523–1371, USA.

*To whom correspondence should be addressed. E-mail: lawtonr@email.uah.edu